Tumor-produced aging-associated oncometabolite, methylmalonic acid, promotes cancer-associated fibroblast activation to drive metastatic progression

Zhongchi Li
Weill Cornell Medicine
Vivien Low
Weill Cornell Medicine https://orcid.org/0000-0002-8561-011X
Valbona Luga
Weill Cornell Medicine
Janet Sun
Weill Cornell Medicine
Ethan Earlie
Weill Cornell Medicine
Bobak Parang
Weill Cornell Medicine
Kripa Shobana Ganesh
Weill Cornell Medical College
Sungyun Cho
Weill Cornell Medical College
Jennifer Endress
Weill Cornell Medical College
Tanya Schild
Weill Cornell Medicine
Menying Hu
Weill Cornell Medicine https://orcid.org/0000-0002-0358-6014
David Lyden
Weill Cornell Medical College https://orcid.org/0000-0003-0193-4131
Wenbing Jin
Weill Cornell Medicine
Chun-Jun Guo
WCMC
Noah Dephoure
Weill Cornell Medicine https://orcid.org/0000-0001-5802-2657
Lewis Cantley

Weill Cornell Medicine https://orcid.org/0000-0002-1298-7653

Ashley Laughney

Weill Cornell Medicine

John Blenis (job2064@med.cornell.edu)

Weill Cornell Medical College https://orcid.org/0000-0003-3622-2337

Article

Keywords:

Posted Date: May 13th, 2022

DOI: https://doi.org/10.21203/rs.3.rs-1643401/v1

Version of Record: A version of this preprint was published at Nature Communications on October 20th, 2022. See the published version at https://doi.org/10.1038/s41467-022-33862-0.

Abstract

The systemic metabolic shifts that occur during aging and the local metabolic alterations of a tumor, its stroma and their communication cooperate to establish a unique tumor microenvironment (TME) that fosters cancer progression. Here, we show that methylmalonic acid (MMA), an aging-increased oncometabolite that is also produced by aggressive cancer cells, activates fibroblasts in the TME, which reciprocally secrete IL-6 loaded extracellular vesicles (EVs) that drive cancer progression, drug resistance and metastasis. The cancer-associated fibroblast (CAF)-released EV cargo is modified as a result of reactive oxygen species (ROS) generation and activation of the canonical and noncanonical TGFβ signaling pathways in CAFs. EV-associated IL-6 functions as a stroma-tumor messenger that activates the JAK/STAT3 and TGFβ signaling pathways in tumor cells and promote an epithelial-to-mesenchymal transition (EMT) and drug resistance *in vitro*, and metastatic progression *in vivo*. Our findings reveal the role of MMA in the activation of CAFs to drive metastatic reprogramming, unveiling multiple potential therapeutic avenues to target MMA at the nexus of aging, the tumor microenvironment and metastasis.

Introduction

Metastasis underlies mortality in the majority of solid-cancer tumors, including lung cancer, the leading cause of cancer death, and melanoma, in which the 5-year survival rate is less than 15% in patients with metastatic disease(1). As a problem of aging, metastasis is the number one cause of death in people 60–79 years old and represents a direct avenue to steer interventions for improving cancer survival and extending overall lifespans(2). Towards this end, much investigative effort continues to focus on mutational, epigenetic, and metabolomic changes within the cancer cell that abet the metastatic process. In this arena, we discovered that methylmalonic acid (MMA), a byproduct of propionate metabolism, is increased in the serum of elderly people and contributes to acquisition of aggressive properties in tumor cells, uncovering a systemic cause for the link between old age and negative cancer outcomes. In addition to the age-dependent increase in circulatory methylmalonic acid, we have more recently also demonstrated that tumor cells dysregulate propionate metabolism in order to increase local MMA accumulation, driving cancer progression in an autocrine manner(3).

Considering that MMA is increased both in the aging body and locally through tumor production, the next question was how these high local concentrations of MMA could function in a paracrine fashion. The influence of the tumor microenvironment (TME) on metastatic progression is inextricable from the equation. Within the heterogeneous and dynamic TME network, the exchange of secreted factors such as hormones, enzymes, growth factors, cytokines and metabolites all facilitate a cooperative tumorigenic and metastatic process between tumor and stroma(4). CAFs represent critical players in the formation of a favorable TME for cancer progression. In addition to extracellular matrix (ECM) deposition and remodeling, CAFs secrete cytokines, growth factors, and metabolites that influence the behavior and function of tumor cells as well as other stromal components. The concentrations, combinations and efficacy of these secreted molecules can be specifically regulated by their delivery through extracellular vesicles, although the mechanisms controlling these parameters are not fully understood (5). In tumor

cells, CAF-secreted messengers influence tumor growth, metastasis and drug resistance through multiple underlying processes, including inhibiting apoptosis pathways, induction of stemness programs, or epithelial-to-mesenchymal transition (EMT) (6, 7). Many of the traits that epithelial-like tumor cells acquire through EMT enhance successful remodeling of their surrounding ECM, support invasion through tissue, and promote intravasation across the endothelial barrier into the bloodstream. This is supported by histopathological studies showing that cells at the invasive front of tumors exhibit an EMT phenotype (8, 9).

In the present study, we show that MMA, increased in the TME by aging as well as by tumor production, activates stromal fibroblasts to cancer-associated fibroblasts (CAFs) and induces a secretory phenotype. In turn, extracellular vesicles (EVs) secreted by MMA-induced CAFs, harboring IL-6 and other factors, promote an epithelial-to-mesenchymal transition in tumor cells, fostering the acquisition of aggressive traits including drug resistance and increased metastatic formation.

Results

MMA secreted from tumor cells activates fibroblasts in the tumor microenvironment

Aberrations in the enzymes downstream of methylmalonyl-CoA in the propionate metabolism pathway, namely methylmalonyl-CoA mutase (*MUT*), methylmalonyl-CoA epimerase (MCEE), methylmalonic aciduria type A protein (*MMAA*), or cob(I)yrinic acid a,c-diamide adenosyl-transferase (*MMAB*) result in pathogenic systemic MMA accumulation in methylmalonic acidemias (10–13), and drive cancer drug resistance and metastasis through increased MMA accumulation *in vitro* and *in vivo*(3)(Fig. 1a). We profiled the transcripts of these metabolic enzymes in individual cells obtained from resected human lung cancer primary tumors and metastases, and found that tumor cells with reduced expression of these genes were enriched in mesenchymal subpopulations (Fig. 1a, 1b). Given this, and our previous findings that metastatic inducers drive MMA production and pro-aggressive effects on tumors through dysregulation of propionate metabolism, we wondered if tumor-produced MMA might also act on other cell types in the TME(3). Fibroblasts comprise the major component of the TME, and in some solid tumors even outnumber malignant cells(14). We knocked down *MUT* in A549 lung carcinoma and A375 melanoma cells to simulate MMA accumulation by altered propionate metabolism during early steps of metastasis, and co-cultured these cells with MRC5 lung and BJ dermal fibroblasts, respectively (Fig. 1c-e). Five days of co-culture markedly increased CAF markers in the fibroblasts, suggesting that tumor-produced MMA is secreted and activates fibroblasts in the stroma (Fig. 1f). Conversely, blocking MMA production in A375 cells by knockdown of *PCCA*, a component of propionyl-CoA-carboxylase, repressed their ability to induce the activation and infiltration of fibroblasts in the tumor *in vivo* (Figure s1a-c). Notably, an RNA-sequencing dataset of 501 whole tumors from patient lung squamous cell carcinomas showed a correlation between low *MUT, MCEE, MMAA* and *MMAB* levels (indicating high MMA) and high expression of cancer-associated fibroblast markers *ACTA1* (encoding for SMA) and *FAP* (Figure s1d),

suggesting that human tumors with greater levels of MMA do indeed harbor a great proportion of inflammatory CAFs.

We have previously demonstrated that MMA in the serum is largely encapsulated in lipid vesicles, allowing for accelerated entry into cells at much lower concentrations compared to free MMA (15). When we isolated extracellular lipid vesicles from the conditioned media of *MUT*-knocked down tumor cells ($EVs^{sh\,MUT-A549}$), we found that they indeed carried more MMA compared to control vesicles ($EVs^{sh\,GFP-A549}$), and could induce CAF markers when used to treat fibroblasts (Figure s1e-f). Depletion of these vesicles from the conditioned media of *MUT*-knocked down cells abolished its ability to induce CAF markers in fibroblasts, confirming that tumor-produced MMA, like the MMA in the serum of elderly people, is delivered and acts on cells through extracellular vesicles (Figure s1g).

Treatment of MRC-5 and BJ fibroblasts with exogenous MMA reproduced the effect of co-culture with or extracellular vesicles from *MUT*-knockdown tumor cells on CAF marker expression in a dose-dependent manner (Fig. 1g). The ability of exogenous MMA to induce CAF markers in fibroblasts was similar to that of the conditioned media and lipid vesicles from *MUT*-knocked down tumor cells, as well as other known CAF inducers, including TGFβ (Figure s1h). Proliferation was not affected by 1mM MMA treatment, and mildly decreased under 5mM of MMA (Figure s1i). We confirmed that MMA activation of CAFs was not simply due to decreased pH or altered TCA cycle flux, as other acids from the propionate metabolism pathway were unable to reproduce the phenotype (Figure s1j). Intriguingly, MMA also induced CAF production of matrix metalloproteinases (Fig. 1f), which contribute to the extracellular matrix (ECM) remodeling that promotes intravasation of tumor cells into the bloodstream in early stages of metastasis (16).

MMA-treated fibroblasts secrete EVs to promote pro-aggressive reprogramming in tumor cells

To determine if the secretome of MMA-activated CAFs might direct tumor cell behavior, we cultured tumor cells with conditioned media from vehicle- or MMA-treated fibroblasts ($CM^{veh-MRC5/BJ}$ and $CM^{MMA-MRC5/BJ}$) and observed a marked increase in markers of EMT (Fig. 2a). Additionally, co-injection of A549 tumor cells with MMA-treated MRC5 fibroblasts into mice significantly increased the ability of tumor cells to metastasize, indicating that one or more secreted factors from MMA-activated CAFs promotes a pro-metastatic phenotype in cancer cells (Fig. 2b).

Next, we aimed to identify the components of the conditioned media secreted by MMA-treated fibroblasts that was driving the EMT phenotype in tumor cells. EVs are loaded with signaling molecules and genetic material, and function as essential signaling mediators in the tumor microenvironment (17, 18). Considering that MMA is delivered from tumor cells to fibroblast in EVs, we looked to see whether the fibroblast messengers reciprocally driving EMT in tumor cells were also contained in EVs. From MRC-5 lung and BJ dermal fibroblasts, we isolated EVs from the conditioned media after vehicle or MMA treatment ($EVs^{veh-MRC5}$ and EVs^{veh-BJ}, or $EVs^{MMA-MRC5}$ and EVs^{MMA-BJ}, respectively) (Fig. 2c). We did not observe a significant difference in the number or size of EVs secreted by MMA-treated fibroblasts ($EVs^{MMA-MRC5/BJ}$) compared to those secreted by vehicle-treated fibroblasts ($EVs^{veh-MRC5/BJ}$) (Figure S2a-

b). Survey of extracellular vesicle marker proteins confirmed the purity of these EVs (Figure S2c). To determine if the CAF-secreted factor driving EMT in tumor cells was being delivered through these structures, we then added $EVs^{veh-MRC5/BJ}$ or $EVs^{MMA-MRC5/BJ}$ to their tissue-matched A549 or A375 tumor cells (Fig. 2c). Upon treatment of tumor cells with $EVs^{MMA-MRC5}$, we once again observed an increase in EMT markers (Fig. 2d). In contrast, the supernatant from the $CM^{MMA-MRC5/BJ}$ after isolation of the EVs lost its ability to induce this effect (Figure S3a). Intriguingly, when A549 tumor cells treated with isolated $EVs^{MMA-MRC5}$ were then cultured in normal media, they converted back to an epithelial phenotype after five days, highlighting the plasticity of EMT (Figure S3b). Importantly, when $EVs^{MMA-MRC5}$-treated tumor cells were released from $EVs^{MMA-MRC5}$ treatment, but subsequently co-cultured in the presence of untreated fibroblasts, the tumor cells maintained their aggressive phenotype (Figure S3b). This underscores the importance of a positive feedback loop between the tumor and stroma, wherein fibroblast activation drives tumor cell aggression, which reciprocally drives more fibroblast activation, ultimately leading to metastatic progression. A375 and A549 tumor cells treated with $EVs^{MMA-MRC5/BJ}$ also exhibited increased resistance to chemotherapeutic and targeted therapy drugs, and displayed increased colony formation in soft agar compared to tumor cells treated with $EVs^{veh-MRC5/BJ}$ (Fig. 2e and 2f). Additionally, tumor cells treated with $EVs^{MMA-MRC5/BJ}$ exhibited increased invasion and migration ability in transwell assays, and formed more metastases following a subcutaneous primary tumor implantation *in vivo* (Fig. 2g, 2h). Intriguingly, despite having significantly higher metastases formation, tumor cells treated with $EVs^{MMA-MRC5}$ did not form significantly larger primary tumors (Fig. 2h). This indicates that the EVs isolated from MMA-activated fibroblasts specifically drive an aggressive, metastatic phenotype in tumor cells, rather than increased cell proliferation.

IL-6 in fibroblast-secreted EVs mediates tumor cell metastatic signaling

As we did not see a change in the number and size of EVs induced by MMA treatment, we speculated that the potent tumor cell response observed after MMA treatment could be due to differentially loaded EV cargo. To identify the active factor in EVs from MMA-treated fibroblasts driving metastatic progression, we performed proteomic analysis on $EVs^{veh-MRC5}$ and $EVs^{MMA-MRC5}$. One of the most significantly upregulated secreted proteins in $EVs^{MMA-MRC5}$ compared to $EVs^{veh-MRC5}$ was IL-6, a pro-inflammatory cytokine that has been implicated in promoting EMT and metastasis (Fig. 3a, Figure s4a) (19–21). We also observed that genes driving IL-6/JAK/STAT3 pathway activity were enriched in more mesenchymal cells characterized by downregulation of key genes restricting MMA production from human lung cancer tumor and metastasis tissue samples (Figure S4b). Indeed, both IL-6/JAK/STAT3 signaling, measured by JAK2 and STAT3 phosphorylation, and TGFβ signaling, measured by phosphorylation of SMAD proteins, were activated in A549 cells upon treatment with EVsMMA-MRC5 (Fig. 3b). Notably, while $EVs^{MMA-MRC5}$ increased Y705 phosphorylation of STAT3, which is the main regulator of cytokine-induced JAK/STAT3 signaling, it did not affect phosphorylation at S727 (Fig. 3b), suggesting a specificity in $EVs^{MMA-MRC5}$ mediated downstream signaling. To determine the necessity of these signaling cascades for the ability of $EVs^{MMA-MRC5}$ to drive EMT, we blocked their activation in A549 tumor cells using the TGFβR or STAT-3

inhibitors, SB431542 and cryptotanshinone, respectively (Fig. 3c). Inhibition of these pathways effectively blocked EMT induction by $EVs^{MMA-MRC5}$ in A549 tumor cells, re-sensitized cells to drug treatment, and suppressed the increase in invasion and migration (Fig. 3d-f). Similarly, knockdown of *IL6R* in tumor cells suppressed both IL-6/JAK/STAT3 and TGFβ signaling, and suppressed $EVs^{MMA-MRC5}$-induced EMT marker expression, drug resistance, and invasion and migration, suggesting that IL-6R activation functions upstream of TGFβ pathway signaling in this context (Fig. 3g-j, Figure S4c). Additionally, treating A549 lung tumor cells with tocilizumab, an IL-6R antibody and inhibitor, replicated the effect of IL-6R knockdown, effectively blocking IL-6/JAK/STAT3 and TGFβ signaling and suppressing the induction of EMT and drug resistance by $EVs^{MMA-MRC5}$ (Figure S4d-f). Finally, we knocked down *IL6* in MRC-5 fibroblasts before treating them with MMA and isolated their secreted EVs. While IL-6 knockdown in fibroblasts did not have any effect on the ability of MMA to induce CAF marker expression in fibroblasts, it effectively suppressed the ability of $EVs^{MMA-MRC5}$ to induce IL6/JAK/STAT3 and TGFβ signaling in tumor cells, and was sufficient to abolish the EMT-inducing effect of $EVs^{MMA-MRC5}$ and their ability to boost drug resistance, invasion and migration (Figure s5).

MMA activates fibroblasts through ROS activated NF-κB and TGFβ signaling

Next, we set out to characterize the mechanism by which MMA treatment of fibroblasts led to activation of the CAF phenotype and IL-6 loading into and secretion from extracellular vesicles. We performed RNA-seq on MRC-5 fibroblasts treated with vehicle or MMA, and a pathway enrichment analysis of the RNA-seq data showed an upregulation of genes in the NF-κB and TGFβ signaling pathways in MMA-treated fibroblasts (Fig. 4a). Crosstalk between these two pathways has been described previously, wherein TGFβ signaling leads to the sequential phosphorylation of TAK1, IKK, and NF-κB (Fig. 4b)(22). We confirmed that these pathways are activated in MRC-5 fibroblasts upon MMA treatment, or treatment by EVs derived from MMA-producing tumor cells ($EVs^{sh\mathit{MUT}-A549}$) (Fig. 4c, s6a). Using time course analysis, we noted that p65 phosphorylation occurred later than SMAD3 and TAK1 phosphorylation (Fig. 4c). Pharmacological inhibition of TGFβR using SB43152, but not of TAK1 and IKK using Takinib and IKK16, respectively, effectively suppressed the induction of CAF markers by MMA, suggesting that the MMA-induced CAF phenotype is largely regulated by TGFβ separately from NF-κB signaling (Fig. 4d-e). Similarly, genetic knockdown of *TGFBR1*, but not *CHUK1* (encoding for IKK1), negated the ability of MMA to induce CAF markers (Figure s6b-c). Interestingly, pharmacological inhibition of TGFβR, TAK1 and IKK were all individually able to reduce IL-6 loading into $EVs^{MMA-MRC5}$, indicating that MMA-induced IL-6 secretion through extracellular vesicles is mediated by NF-κB downstream of TGFβ-TAK1-IKK activation, and we saw the same effect with genetic knockdown of *TGBR1* and *CHUK1* (Fig. 4f, s6d-e). In line with this and our earlier findings demonstrating the necessity of IL-6, all three inhibitors abrogated the ability of $EVs^{MMA-MRC5}$ to induce IL-6/JAK/STAT3 and TGFβ signaling in A549 tumor cells, along with EMT (Fig. 4g-h, Figure s6f-g). Additionally, all three inhibitors were able to suppress the ability of $EVs^{MMA-MRC5}$ to increase drug resistance in tumor cells, although this effect was small using SB43152 or TAKinib (Fig. 4i).

Notably, IKK inhibition had a greater effect than both TGFβR inhibition or TAK1 inhibition in reducing IL-6 loading into $EVs^{MMA-MRC5}$, which also corresponded with a greater effect in suppressing the potency of $EVs^{MMA-MRC5}$ for promoting EMT and drug resistance in A549 tumor cells (Fig. 4f-i). This suggested that the NF-κB activation downstream of TGFβR signaling was supplemented by a certain level of NF-κB activation independent of TGFβR signaling, together producing the full effect of IL-6 loading into $EVs^{MMA-MRC5}$ and the full potency of $EVs^{MMA-MRC5}$ to induce EMT and increase drug resistance in tumor cells.

As increased generation of reactive oxygen species (ROS) has been established to trigger both NF-κB and TGFβ signaling(23, 24), we conjectured that ROS activation of NF-κB both independently and through TGFβR-TAK1-IKK-NF-κB signaling may be at the apex of the MMA signal that induces the CAF phenotype and function. Additionally, pathway enrichment analysis of RNA-seq data showed that the oxidative stress response was upregulated in MMA-treated MRC-5 fibroblasts (Fig. 4a). Indeed, MMA treatment, as well as treatment by EVs from MMA-producing tumor cells ($EVs^{sh\,MUT-A549}$) of tumor cells increased ROS with peak levels at 6 hours, corresponding to the peak in TGFβ and NF-κB signaling, while also increasing malondialdehyde (MDA), a marker of oxidative stress, over several days (Fig. 4c, Fig. 5a, Figure s7a-c). While ROS induction by MMA was similar to that observed by other ROS inducers, including rotenone, TTFA, and hydrogen peroxide, these other inducers were unable to drive the same level of CAF activation in the fibroblasts (Figure s7d-e). This suggests that MMA may increase ROS through a specific mechanism, or that MMA activates other processes that work with ROS to induce activation of fibroblasts.

Treatment of these fibroblasts with the antioxidants N-acetyl-cysteine (NAC) or SkQ1 effectively inhibited MMA induction of NF-κB and TGFβ signaling, along with the MMA-induced increase in CAF markers and increased IL-6 loading into $EVs^{MMA-MRC5}$ (Fig. 5b-e). When $EVs^{MMA-MRC5}$ were collected from fibroblasts that were co-treated with antioxidants, they were no longer able to activate IL6/JAK/STAT3 or TGFβ signaling in A549 tumor cells (Fig. 5f). Consistently, antioxidant treatment of fibroblasts suppressed the ability of $EVs^{MMA-MRC5}$ to induce the EMT phenotype and increase drug resistance in A549 tumor cells, and reversed the ability of these tumor cells to form metastases *in vivo* (Fig. 5g-i). Together, our data illustrates a mechanism wherein exposure of fibroblasts to MMA generates ROS and induces oxidative stress, which activates NF-κB and TGFβ signaling. Canonical TGFβ signaling regulates CAF marker expression, while NF-κB signaling, which is activated by ROS both independently of and downstream of TGFβ signaling through TAK1 and IKK, regulates IL-6 association and secretion with vesicles. In tumor cells, IL-6 enriched $EVs^{MMA-MRC5}$ activates IL-6/JAK/STAT3 and TGFβ signaling, promoting EMT and the acquisition of pro-aggressive traits (Fig. 6).

Discussion

Here, we depict how a recently identified aging-associated and tumor-produced oncometabolite, MMA, can also function as a tumor cell messenger by acting on the tumor microenvironment to drive metastatic

progression. We also characterize for the first time the downstream signaling cascades activated by MMA in fibroblasts. By increasing ROS generation, MMA induces a secretory signature in CAFs wherein IL6 delivered in extracellular vesicles drives metastatic signaling and progression of epithelial-like (or primary) cancer cells.

While the structure of the signaling cascades activated by MMA are likely to vary according to cell-type, the ability of MMA to induce oxidative stress may be a conserved phenomenon upstream of MMA-mediated functions in other cellular contexts, such as the TGFβ signaling-dependent increase in SOX4 in MMA-treated tumor cells(15). More research is warranted to verify this possibility, as well as to elucidate how MMA may increase ROS. A potential mechanism may involve MMA's ability to inhibit succinate dehydrogenase, an essential component of the mitochondrial respiratory chain complex II(25). Indeed, diseased mitochondria and mitophagy dysfunction has been described in *MUT* deficiency underlying methylmalonic acidemia(26).

The role of circulatory IL-6 in metastasis and therapy resistance has been previously observed, and is long known to be increased in the serum with age(27, 28). IL-6 was also reported to be increased in the serum of Methylmalonic acidemia patients recently (29).The discovery of a specific mode of IL-6 delivery from TME to stroma through extracellular vesicles, however, likely confers a particularly calibrated and potent effect. The proportion of IL-6 released freely or delivered through EVs has been shown to vary widely and depend on the biological systems involved; for example, almost all IL-6 released from monocytes are free, while all IL-6 released from T cells are encapsulated(30). In addition to providing a concentrated influx of the cytokine when IL-6 is delivered through these lipidic structures, extracellular vesicles also protect their contents from environmental degradation, and expression of surface proteins may facilitate the targeting of EVs to distinct cell types(30). Co-delivery of different cytokines encapsulated together is also likely to have different synergistic effects driving distinct phenotypes. A precise characterization of the regulatory mechanisms dictating how IL-6 is loaded into EVs and the proportions of IL-6 encapsulated or embedded in the membranes will require further investigation, and will likely illuminate key pathways for cytokine delivery through EVs in other cellular contexts.

As IL-6 signaling is pro-inflammatory and TGF-β signaling is anti-inflammatory, their associated pathways are often described to function antagonistically. For example, STAT3 can bind Smad3 and disrupt formation of Smad2/Smad3 complexes, hindering the DNA-binding ability of these transcription factors(31). In contrast, we show that STAT3 signaling in tumor cells treated with $EVs^{MMA-MRC5}$ promotes TGF-β signaling in a positive crosstalk interaction to drive EMT. This is supported by previous studies which found that STAT3-Smad3 complex formation and nuclear translocation is required for TGF-β-induced *Snail* promoter activation and EMT induction in *KRAS* mutated Panc-1 cells(32). The factors that determine the nature of these interactions in different contexts remain to be elucidated and may be defined by the varying strengths of each pathway's activation or by the expression of additional co-factors.

Furthermore, while this was not explored in the current study, our findings support a likely means by which the aging body shapes the tumor microenvironment through MMA, further coloring in the link between age as a risk factor and poorer cancer outcomes. Indeed, it has been shown that older people have increased tissue fibrosis, and the possibility that MMA may play a role in this is certainly intriguing (33). Beyond the effect of MMA on fibroblasts, the full scope of how MMA functions on other cell components of the tumor microenvironment, such as the immune system, has yet to be uncovered, and represents a huge untapped potential for therapeutic interventions targeting various stages of the tumorigenic process.

Declarations

Contributions

Z.L., V. Low, and J.B. conceived and supervised the project. Z.L. and V. Low. performed most of the cell culture, molecular biology experiments, the EMT-related experiments, the invasion and migration experiments, drug resistance and the mouse experiments. V. Low. prepared the RNA for RNA-seq, generated the viral particles for knockdowns, generated the genetically modified cell lines, and performed qPCR analyses. E.E and A.L performed patient single cell data analysis. M.H. performed EVs quantification by Nano Sight. J.S. and V. Luga performed Electron Microscopy analysis of EVs and quantification of particle size. W.J. and C.-J.G. performed metabolomic analysis. N.D. performed proteomic analysis. K.G. assisted in data analysis. B.P., J. E., S.C. and T.C. assisted in some cell culture and molecular experiments. Z.L., V. Low., and J.B. analyzed the data. The manuscript was written by Z.L., V. Low. and J.B., and edited by A.L. and V. Luga. All authors discussed the results and approved the manuscript.

Acknowledgements

We are grateful to members of the Blenis and Cantley Laboratories for critical input on this project. Elena Piskounova kindly provided luciferase plasmid for xenograft experiments. This research was supported by the following grants: R01GM051405 (J.B.), R01CA46595 (J.B.). C.-J.G. is supported by the AGA Research Foundation, WCM-RAPP Initiative, The. W. M. Keck Foundation, the National Institutes of Health (DP2 HD101401-01). A.L. is funded by R01CA256188-01. V.Luga is funded by Canadian Institutes of Health Research (CIHR) fellowship. The authors acknowledge the assistance of the staff at the Microscopy & Image Analysis Core at WCM. TEM was purchased with funds from an NIH Shared Instrumentation Grant (S10RR027699)".

References

1. A. Sandru, S. Voinea, E. Panaitescu, A. Blidaru, Survival rates of patients with metastatic malignant melanoma. J Med Life **7**, 572–576 (2014).
2. R. L. Siegel, K. D. Miller, A. Jemal, Cancer statistics, 2018. CA Cancer J Clin **68**, 7–30 (2018).

3. A. P. Gomes *et al.*, Altered propionate metabolism contributes to tumour progression and aggressiveness. Nat Metab, (2022).
4. N. M. Anderson, M. C. Simon, The tumor microenvironment. Curr Biol **30**, R921-R925 (2020).
5. E. Sahai *et al.*, A framework for advancing our understanding of cancer-associated fibroblasts. Nat Rev Cancer **20**, 174–186 (2020).
6. M. E. Fiori *et al.*, Cancer-associated fibroblasts as abettors of tumor progression at the crossroads of EMT and therapy resistance. Mol Cancer **18**, 70 (2019).
7. Y. Chen, K. M. McAndrews, R. Kalluri, Clinical and therapeutic relevance of cancer-associated fibroblasts. Nat Rev Clin Oncol **18**, 792–804 (2021).
8. E. Beerling *et al.*, Plasticity between Epithelial and Mesenchymal States Unlinks EMT from Metastasis-Enhancing Stem Cell Capacity. Cell Rep **14**, 2281–2288 (2016).
9. T. Brabletz *et al.*, Variable beta-catenin expression in colorectal cancers indicates tumor progression driven by the tumor environment. Proc Natl Acad Sci U S A **98**, 10356–10361 (2001).
10. F. Keyfi, M. Sankian, M. Moghaddassian, A. Rolfs, A. R. Varasteh, Molecular, biochemical, and structural analysis of a novel mutation in patients with methylmalonyl-CoA mutase deficiency. Gene **576**, 208–213 (2016).
11. H. Bikker *et al.*, A homozygous nonsense mutation in the methylmalonyl-CoA epimerase gene (MCEE) results in mild methylmalonic aciduria. Hum Mutat **27**, 640–643 (2006).
12. C. M. Dobson *et al.*, Identification of the gene responsible for the cblA complementation group of vitamin B12-responsive methylmalonic acidemia based on analysis of prokaryotic gene arrangements. Proc Natl Acad Sci U S A **99**, 15554–15559 (2002).
13. A. Jorge-Finnigan *et al.*, Functional and structural analysis of five mutations identified in methylmalonic aciduria cblB type. Hum Mutat **31**, 1033–1042 (2010).
14. J. Huelsken, D. Hanahan, A Subset of Cancer-Associated Fibroblasts Determines Therapy Resistance. Cell **172**, 643–644 (2018).
15. A. P. Gomes *et al.*, Age-induced accumulation of methylmalonic acid promotes tumour progression. Nature **585**, 283–287 (2020).
16. J. Winkler, A. Abisoye-Ogunniyan, K. J. Metcalf, Z. Werb, Concepts of extracellular matrix remodelling in tumour progression and metastasis. Nat Commun **11**, 5120 (2020).
17. F. Wendler *et al.*, Extracellular vesicles swarm the cancer microenvironment: from tumor-stroma communication to drug intervention. Oncogene **36**, 877–884 (2017).
18. V. Luga *et al.*, Exosomes mediate stromal mobilization of autocrine Wnt-PCP signaling in breast cancer cell migration. Cell **151**, 1542–1556 (2012).
19. J. Gyamfi, Y. H. Lee, M. Eom, J. Choi, Interleukin-6/STAT3 signalling regulates adipocyte induced epithelial-mesenchymal transition in breast cancer cells. Sci Rep **8**, 8859 (2018).
20. T. Ara *et al.*, Interleukin-6 in the bone marrow microenvironment promotes the growth and survival of neuroblastoma cells. Cancer Res **69**, 329–337 (2009).

21. R. Salgado *et al.*, Circulating interleukin-6 predicts survival in patients with metastatic breast cancer. Int J Cancer **103**, 642–646 (2003).
22. C. Freudlsperger *et al.*, TGF-beta and NF-kappaB signal pathway cross-talk is mediated through TAK1 and SMAD7 in a subset of head and neck cancers. Oncogene **32**, 1549–1559 (2013).
23. M. J. Morgan, Z. G. Liu, Crosstalk of reactive oxygen species and NF-kappaB signaling. Cell Res **21**, 103–115 (2011).
24. R. M. Liu, L. P. Desai, Reciprocal regulation of TGF-beta and reactive oxygen species: A perverse cycle for fibrosis. Redox Biol **6**, 565–577 (2015).
25. J. C. Dutra *et al.*, Inhibition of succinate dehydrogenase and beta-hydroxybutyrate dehydrogenase activities by methylmalonate in brain and liver of developing rats. J Inherit Metab Dis **16**, 147–153 (1993).
26. A. Luciani *et al.*, Impaired mitophagy links mitochondrial disease to epithelial stress in methylmalonyl-CoA mutase deficiency. Nat Commun **11**, 970 (2020).
27. W. B. Ershler *et al.*, Interleukin-6 and aging: blood levels and mononuclear cell production increase with advancing age and in vitro production is modifiable by dietary restriction. Lymphokine Cytokine Res **12**, 225–230 (1993).
28. N. Kumari, B. S. Dwarakanath, A. Das, A. N. Bhatt, Role of interleukin-6 in cancer progression and therapeutic resistance. Tumour Biol **37**, 11553–11572 (2016).
29. Q. Li *et al.*, Determination of Cytokines and Oxidative Stress Biomarkers in Cognitive Impairment Induced by Methylmalonic Acidemia. Neuroimmunomodulation, 1–9 (2021).
30. W. Fitzgerald *et al.*, A System of Cytokines Encapsulated in ExtraCellular Vesicles. Sci Rep **8**, 8973 (2018).
31. G. Wang *et al.*, STAT3 selectively interacts with Smad3 to antagonize TGF-beta signalling. Oncogene **35**, 4422 (2016).
32. M. Saitoh *et al.*, STAT3 integrates cooperative Ras and TGF-beta signals that induce Snail expression. Oncogene **35**, 1049–1057 (2016).
33. L. A. Murtha *et al.*, The Role of Pathological Aging in Cardiac and Pulmonary Fibrosis. Aging Dis **10**, 419–428 (2019).

Figures

Figure 1

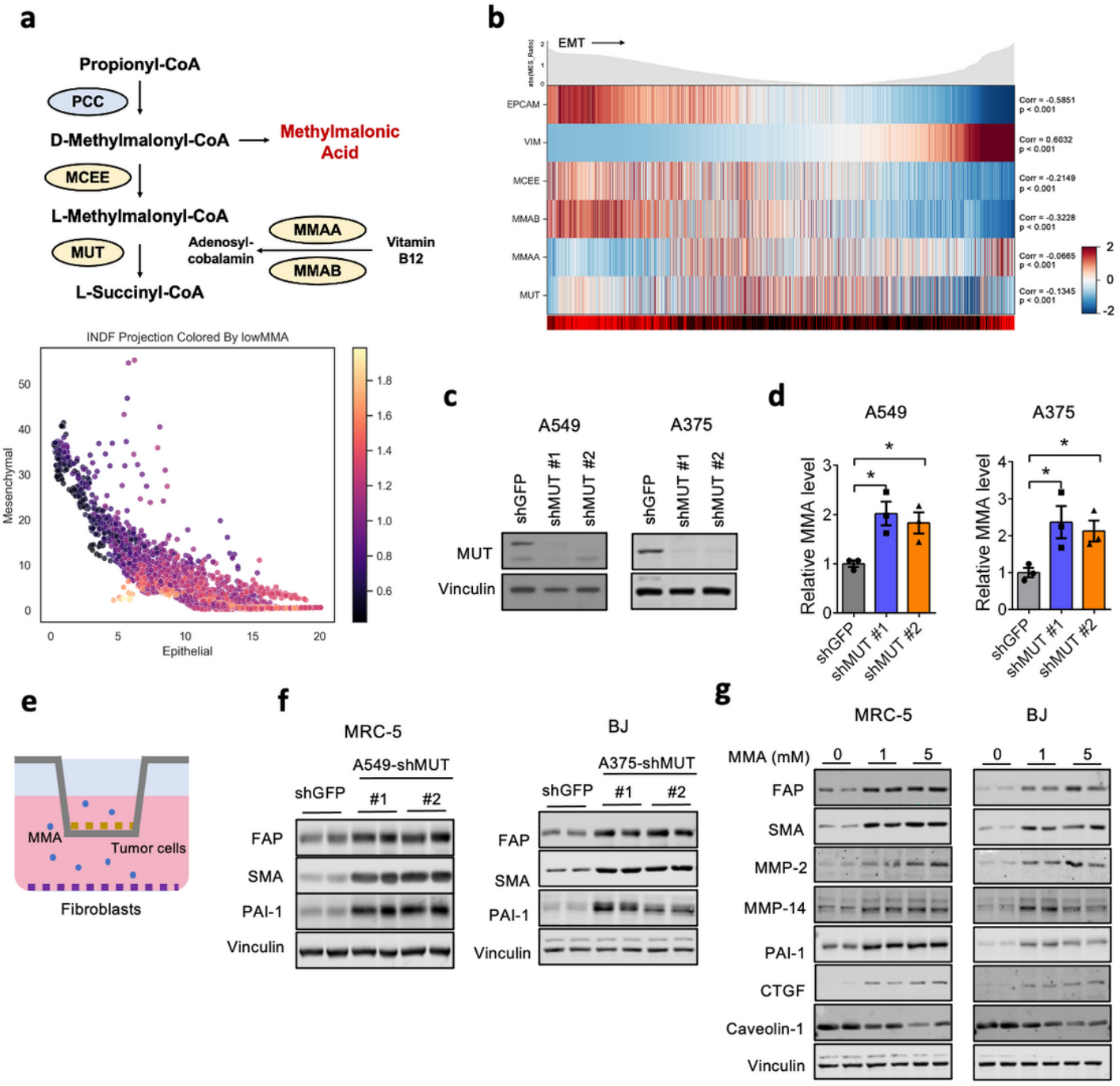

Figure 1

MMA produced by tumor cells promotes a cancer associated fibroblast phenotype. a. Patient-derived tumor cells (n = 2,537) projected according to imputed Vimentin expression and imputed EPCAM expression. Each cell is colored by average imputed expression of negative regulators of MMA production (MMAA, MMAB, MCEE, and MUT), highlighted in yellow in the diagram depicting propionate metabolism pathway (above). **b.** The z-normalized imputed expression of relevant mesenchymal, epithelial, and MMA

marker genes is displayed on the heat map ranked by MES Ratio, defined as the log10 transform of the expression ratio of imputed VIM and EPCAM for each cell. The MES Ratio curve along the top of the heat map shows the absolute value of the MES Ratio across the ranked cells. The color bar along the bottom of the heat map shows the sample tissue source (metastasis: red and primary: black). The gene correlation and associated p-values were computed by performing a two-sided spearman test between the normalized (non-imputed) expression of each gene and the MES Ratio. **c.** MUT was knocked down in A549 and A375 tumor cells. Immunoblots show the protein level of MUT in cell lysates. **d**. MMA levels in the conditioned medium of the tumor cells were measured, normalized to the total cell number (n=3 independent experiments, two-sided paired t-test, * p<0.05). **e**. Schematic of the co-culture experiment performed in (**f**). Tumor cells with sh*GFP* or sh*MUT* knockdown were seeded in a transwell insert, and co-cultured with fibroblasts seeded on the bottom of 6-well plates. Fibroblast lysates were collected for immunoblots. **f.** Immunoblots measuring CAF markers in MRC-5 fibroblasts co-cultured for 4 days with sh*MUT*-knocked down A549 tumor cells and BJ fibroblasts co-cultured for 4 days with sh*MUT*-knocked down A375 tumor cells. **g.** Immunoblots measuring CAF markers in MRC-5 and BJ cell lysates treated with 1mM or 5mM of MMA for 5 days.

Figure 2

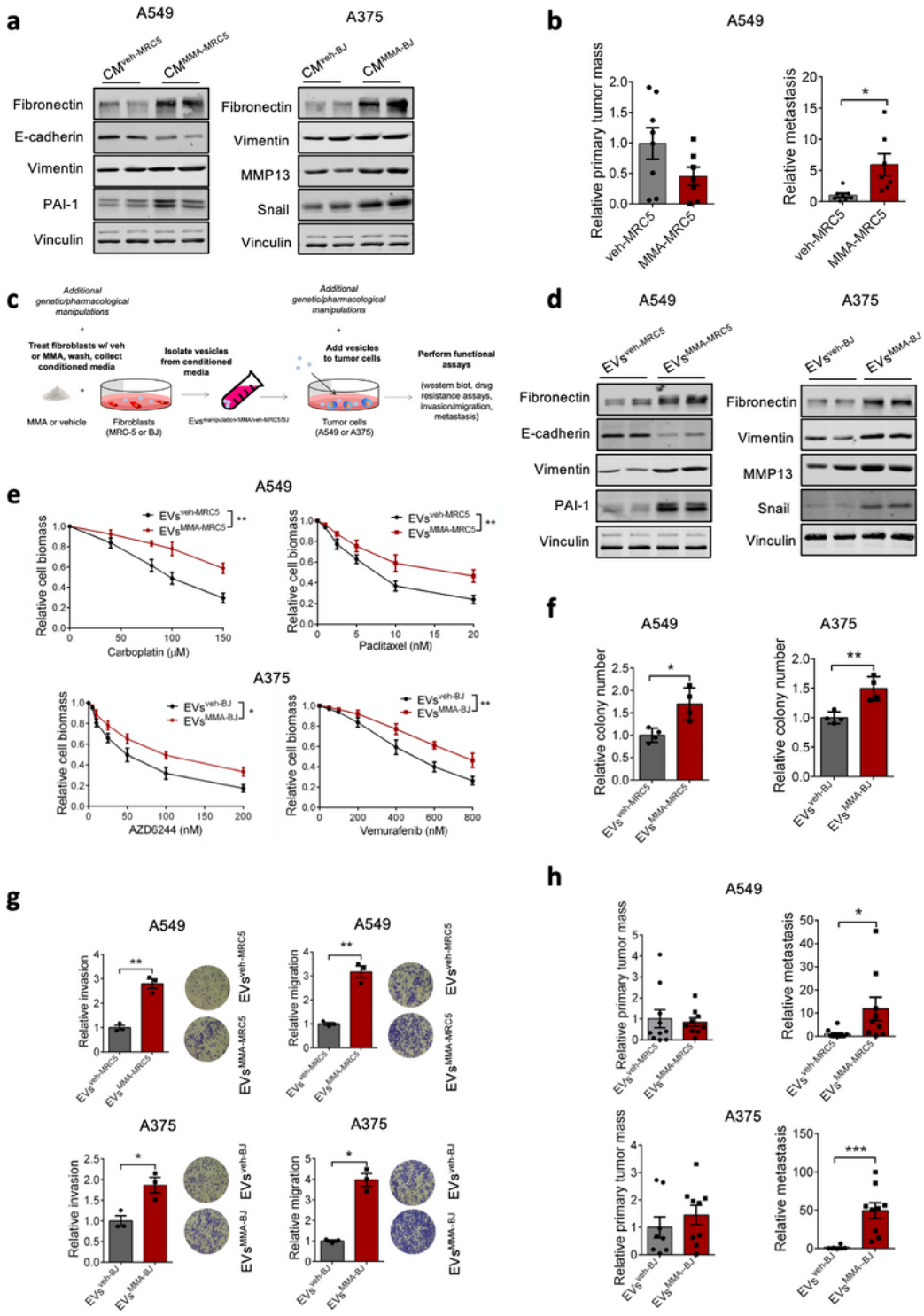

Figure 2

EVs secreted by MMA-treated fibroblasts increase tumor aggressiveness. a. Immunoblots of A549 and A375 tumor cells after 5-day treatment by conditioned media from vehicle or MMA-treated MRC-5 (for A549) or BJ (for A375) fibroblasts. **b.** A mixture of vehicle- or MMA-treated MRC5 with A549 cells were injected subcutaneously. The primary tumor and metastasis formation was measured after 6 weeks (n=7-8, two-sided unpaired t-test, * p<0.05). **c**. Experimental scheme. **d-f.** Pro-aggressive properties in A549 and

A375 tumor cells treated with $EVs^{veh\text{-}MRC5/BJ}$ or $EVs^{MMA\text{-}MRC5/BJ}$ from MRC-5 (for A549) or BJ fibroblasts (for A375), evaluated by immunoblots measuring EMT marker expression (**d**), drug resistance assays using carboplatin and paclitaxel for A549 cells, and vemurafenib and AZD6244 for A375 cells (**e;** n=3 independent experiments, two-way ANOVA, * $p<0.05$, ** $p<0.01$), colony formation assays for 3 weeks (**f;** n = 4 independent experiments, two-sided paired t-test, * $p<0.05$, ** $p<0.01$), transwell invasion and migration assays (**g;** n=3 independent experiments, two-sided paired t-test, * $p<0.05$, ** $p<0.01$) and measurement of primary tumor and metastasis formation 5 weeks after subcutaneous injection into mice (**h**; n=8-10, two-sided unpaired t-test, * $p<0.05$, *** $p<0.001$)**.**

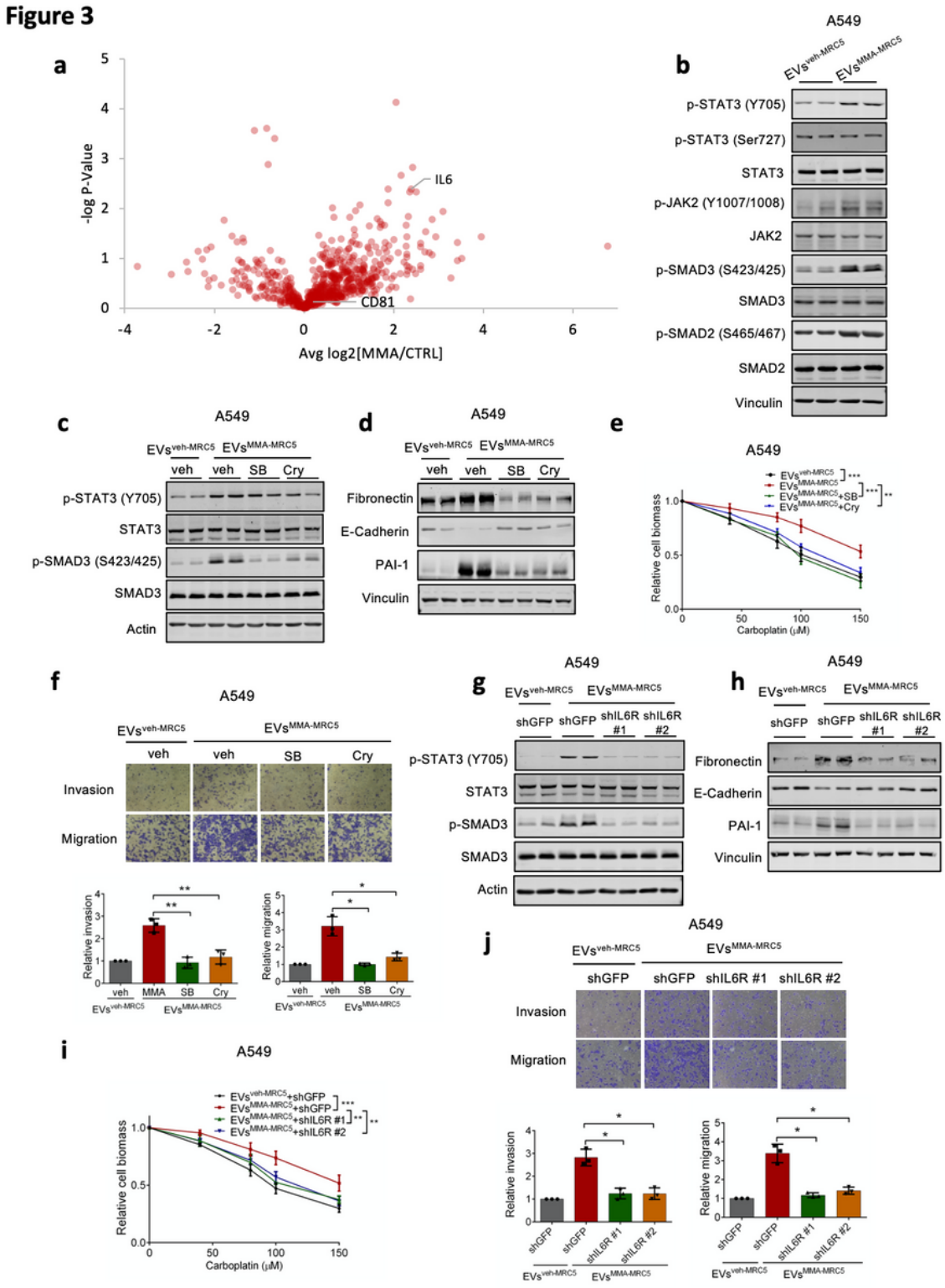

Figure 3

IL-6 in the EVs of MMA-treated fibroblasts mediates pro-aggressive STAT-3 and TGFβ signaling in tumor cells. a. Volcano plots showing protein level distribution from proteomics analysis comparing the compositions of EVs isolated from vehicle- or MMA-treated MRC-5 fibroblasts. **b.** Immunoblots showing JAK2-STAT3 signaling and TGFβ signaling after 3 hours of EV treatment in A549 cells. **c.** Immunoblots measuring signal activation in A549 cells pre-treated with vehicle, TGFβR inhibitor SB431542 or JAK

inhibitor cryptotanshinone for 30 minutes, then treated with EVs from MRC-5 fibroblasts for 3 hours. **d, e, f.** Pro-aggressive properties of A549 cells treated with $EVs^{veh\text{-}MRC5}$ or $EVs^{MMA\text{-}MRC5}$ with or without the TGFβR inhibitor SB431542 or the JAK inhibitor cryptotanshinone for 4 days, evaluated by immunoblots measuring EMT marker expression (**d**), carboplatin resistance assay (**e**; n=3 independent experiments, two-way ANOVA, ** p<0.01, *** p<0.001), and invasion and migration transwell assays (**f;** n=3 independent experiments, two-sided paired t-test, * p <0.05, ** p <0.01). **g.** Immunoblots measuring signal activation in A549 cells with sh*GFP* or *shIL-6R* knockdown (#1 and #2) and treated with $EVs^{veh\text{-}MRC5}$ or $EVs^{MMA\text{-}MRC5}$ for 3 hours. **h, i, j.** Pro-aggressive properties of A549 cells treated with of $EVs^{veh\text{-}MRC5}$ or $EVs^{MMA\text{-}MRC5}$ with sh*GFP* or *shIL-6R* knockdown for 5 days, evaluated by immunoblots measuring EMT marker expression (**h**), carboplatin resistance assay (**i**; n=3 independent experiments, two-way ANOVA, ** p<0.01, **** p<0.0001), and invasion and migration transwell assays (**j;** n=3 independent experiments, two-sided paired t-test, * p<0.05, ** p<0.01).

Figure 4

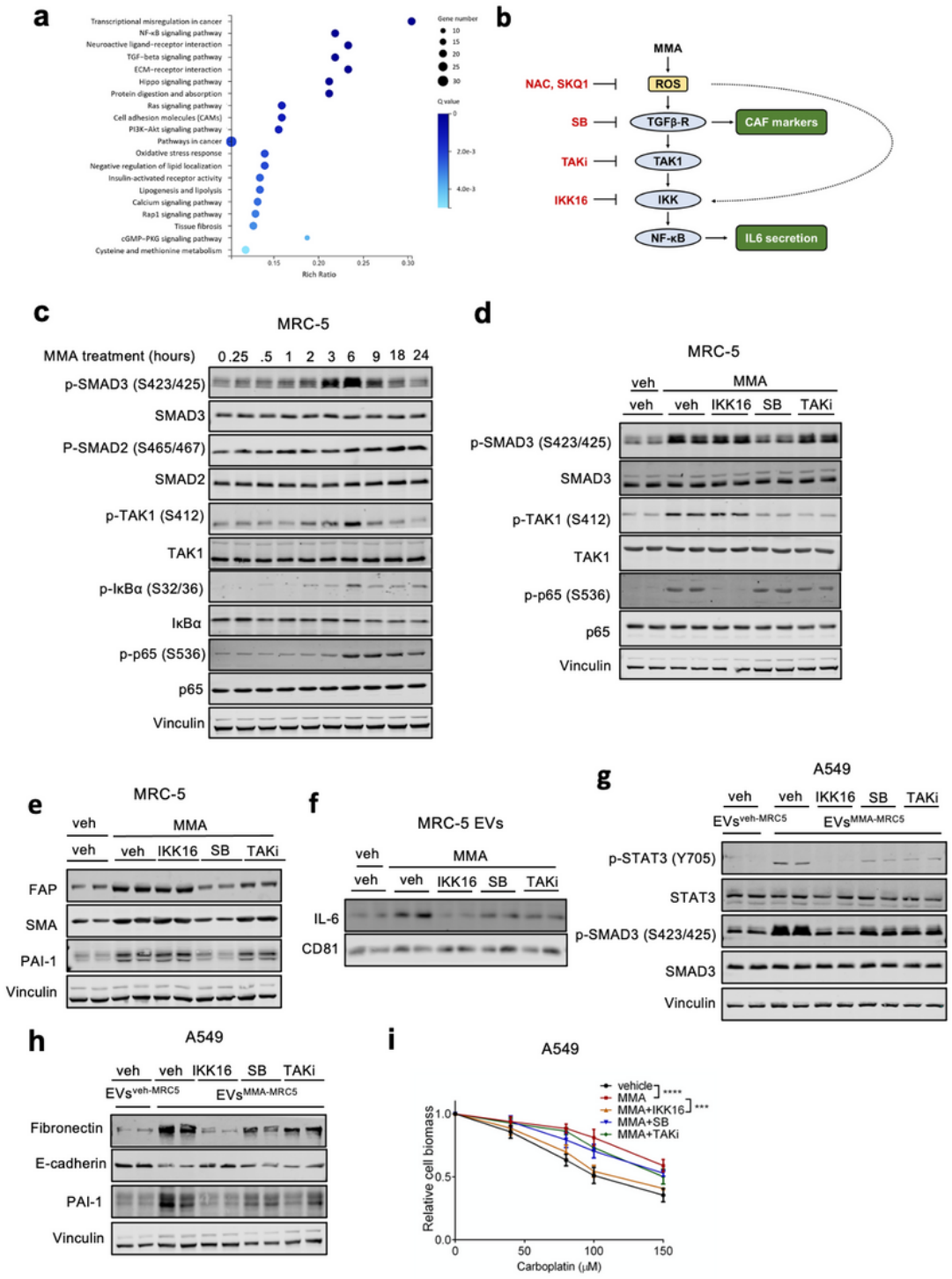

Figure 4

MMA promotion of the CAF phenotype and EV-associated IL6 secretion occurs through TGF-β and NF-κB signaling. a. Pathway enrichment analysis on RNA-seq data from MRC-5 cells treated with vehicle or MMA for 5 days. Genes with expression differences greater than 2-fold and $p<0.001$ were counted. b. TGFβ signaling leads to downstream NF-κB activation. c. Immunoblots measuring signal activation over time in MRC-5 fibroblasts treated with 1mM MMA. d. Immunoblots measuring signaling activation in

MRC-5 fibroblasts treated with MMA alone or in combination with IKK inhibitor IKK16, TGFβR inhibitor SB431542, or TAK1 inhibitor TAKinib for 6 hours. e. Immunoblots of CAF markers in MRC-5 lysates treated with MMA in combination with IKK inhibitor IKK16, TGFβR inhibitor SB431542, or TAK1 inhibitor TAKinib for 5 days. f. Immunoblots showing IL-6 amount in EVs from MRC-5 fibroblasts treated with vehicle or MMA or MMA alone or in combination with IKK inhibitor IKK16, TGFβR inhibitor SB431542, or TAK1 inhibitor TAKinib. g. Immunoblots measuring signaling activation in A549 cells treated with EVs from MRC-5 fibroblasts treated with MMA alone or in combination with IKK inhibitor IKK16, TGFβR inhibitor SB431542, or TAK1 inhibitor TAKinib for 3 hours. h, i. Pro-aggressive properties of A549 cells treated with EVs from MRC-5 fibroblasts treated with vehicle or MMA or MMA alone or in combination with IKK inhibitor IKK16, TGFβR inhibitor SB431542, or TAK1 inhibitor TAKinib, evaluated by immunoblots measuring EMT marker expression (h) and carboplatin resistance assay (i; n=3 independent experiments, two-way ANOVA, *** $p<0.001$, **** $p<0.0001$).

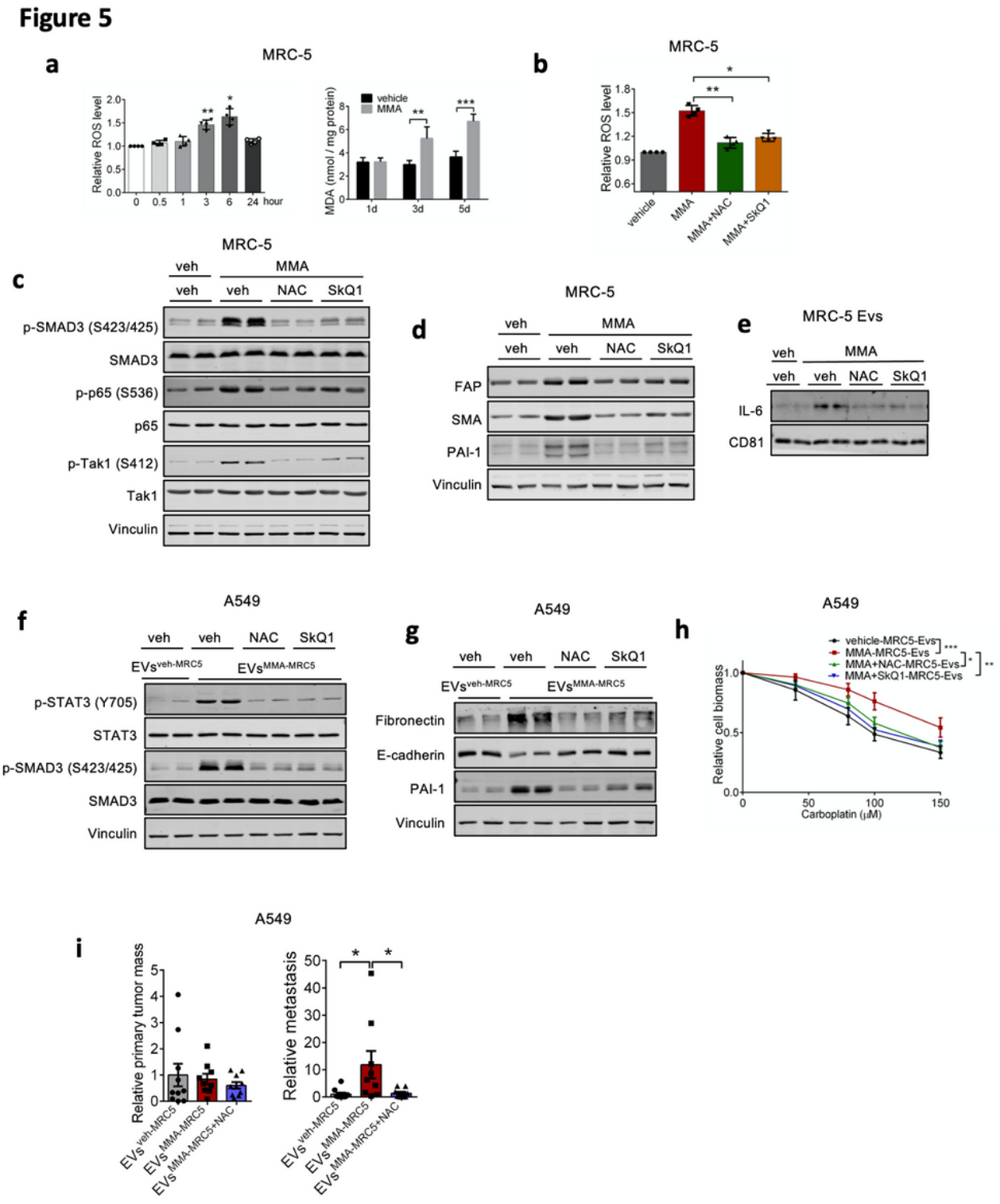

Figure 5

TGF-β and NF-κB mediated activation of fibroblasts and EV-associated IL6 secretion occurs downstream of ROS generation. a. (left) ROS levels and (right) MDA levels in MRC-5 fibroblasts after 1mM MMA treatment (n=4 independent experiments for ROS measurement, one-way ANOVA; n=3 independent experiments for MDA measurement, two-sided paired t-test, * p<0.05, ** p<0.01, *** p<0.001). b. ROS levels in MRC-5 fibroblasts after MMA treatment in combination with NAC or SkQ1(n=4 independent

experiments, two-sided paired t-test, * p<0.05, ** p<0.01). c, d. Immunoblots of MRC-5 fibroblasts treated with MMA alone or in combination with NAC or SkQ1 for 6 hours (c) or 5 days (d). e. immunoblots showing IL-6 amount in EVs from MRC-5 fibroblasts after MMA treatment in combination with NAC or SkQ1. f. Immunoblots measuring signaling activation in A549 cells treated for 3 hours with $EVs^{veh\text{-}MRC5}$ or $EVs^{MMA\text{-}MRC5}$from MRC-5 fibroblasts treated with MMA alone or in combination with NAC or SkQ1. g, h. Pro-aggressive traits of A549 cells treated for 5 days with $EVs^{veh\text{-}MRC5}$ or $EVs^{MMA\text{-}MRC5}$ from MRC-5 fibroblasts treated with MMA alone or in combination with NAC or SkQ1, evaluated by immunoblots measuring EMT marker expression (g) and carboplatin resistance assay (h; n=3 independent experiments, two-way ANOVA, ** p<0.01, *** p<0.001). i. Primary tumor and metastasis formation in mice 4 weeks after subcutaneous injection of A549 cells treated with EVs from MRC-5 fibroblasts treated with vehicle, MMA, or MMA and NAC (n=9-10, two-sided unpaired t-test, * p<0.05). Data is partially previously represented in Figure 2g.

Figure 6

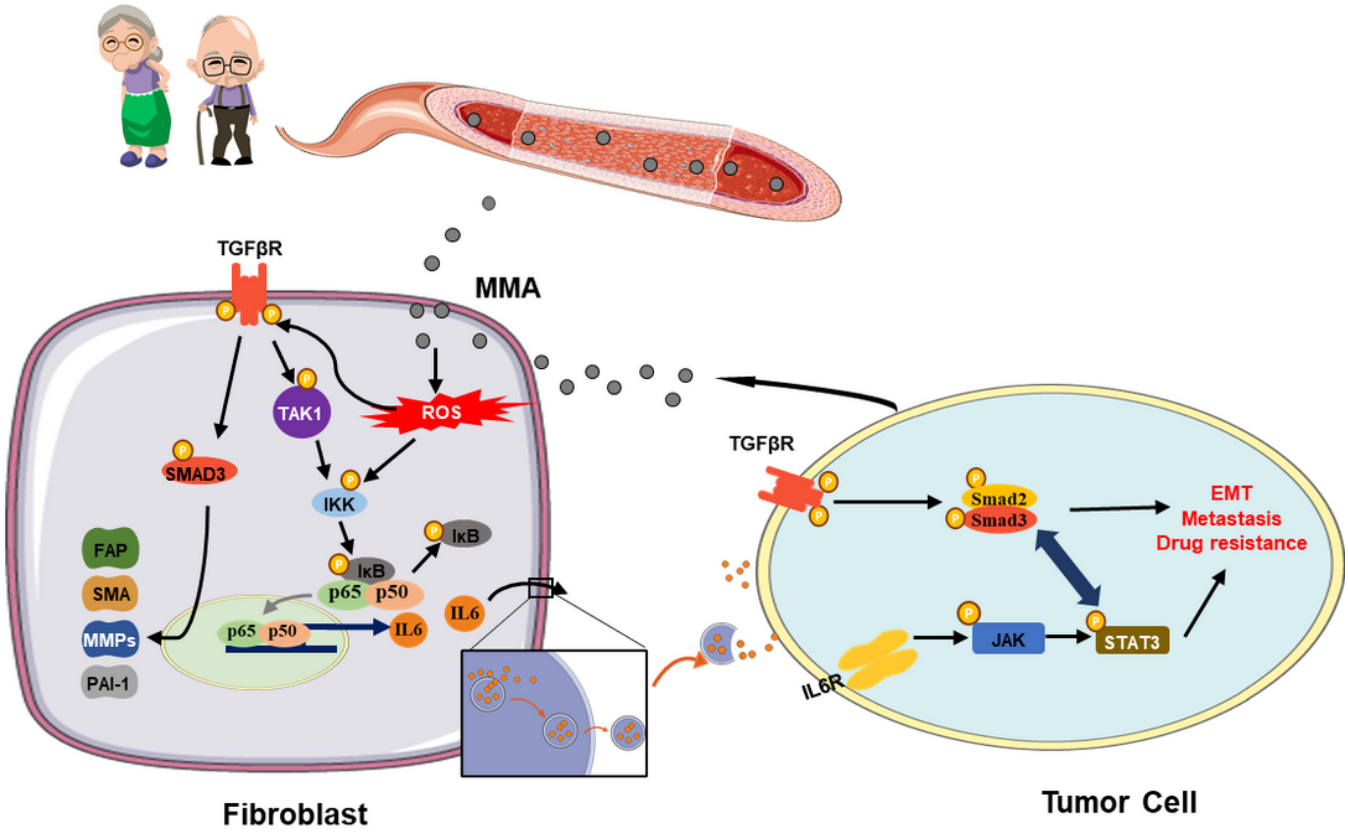

Figure 6

MMA activates fibroblasts and induces their EV-associated IL6 secretion, which drives metastatic reprogramming in tumor cells. MMA produced by tumor cells induces generation of ROS in fibroblasts.

ROS activates TGFβ signaling, which promotes expression of CAF markers, and NF-κB signaling, which promotes IL-6 loading into and secretion through EVs. EVs loaded with IL-6 activate STAT-3 signaling and TGFβ signaling in tumor cells, promoting EMT, drug resistance and metastasis.

Supplementary Files

This is a list of supplementary files associated with this preprint. Click to download.

- MaterialsandMethods202257.docx
- rs.pdf
- nreditorialpolicychecklist.pdf
- supplementarydata2022510VL.docx